Electrochemistry Communications 103 (2019) 31–36

Contents lists available at ScienceDirect

Electrochemistry Communications

journal homepage: www.elsevier.com/locate/elecom

Full communication

Electrodeposition of cobalt thin films and nanowires from ethylene glycol-based solution

Gabriele Panzeri[a], Alessandra Accogli[a], Eugenio Gibertini[a], Sara Varotto[b], Christian Rinaldi[b], Luca Nobili[a], Luca Magagnin[a,*]

[a] Dipartimento di Chimica, Materiali e Ingegneria Chimica Giulio Natta, Politecnico di Milano, 20131 Milano, Italy
[b] Dipartimento di Fisica, Politecnico di Milano, 20133 Milano, Italy

ARTICLE INFO

Keywords:
Organic solvent
Magnetization
Non-aqueous
Electroplating
Alumina template

ABSTRACT

Ethylene glycol-based solutions containing metal precursor chloride salts were investigated for the electrodeposition of cobalt thin films and nanowires. The electrochemical behavior of 0.5 M Co(II) chloride solution at 70 °C was studied by means of cyclic voltammetry (CV) on a Pt substrate. The reduction process was shown to be irreversible, with high faradaic efficiencies (85–90 %). A diffusion coefficient (D_0) of 2.29×10^{-6} cm^2 s^{-1} for the Co species was estimated from the electrochemical behavior at different scan rates (from 25 to 125 mV s^{-1}). The electrodeposition process was also studied on a copper substrate at different cathodic potentials (from −0.75 V vs Pt to −0.95 V vs Pt). Field-emission scanning electron microscopy (FE-SEM) and electron dispersive spectroscopy (EDS) revealed high-purity, compact films. Template-assisted electrodeposition resulted in ~16–18 μm long cobalt nanowires with an aspect ratio $L/D > 100$. X-ray diffraction (XRD) analysis of Co thin films showed a preferential orientation along the HCP [100] direction, which was even more marked for the nanowires. Vibrating sample magnetometry (VSM) highlighted that the fact that Co thin films were magnetized in-plane, while in nanowires a competition between shape and magnetocrystalline anisotropy led to similar magnetic behavior for the in-plane and out-of-plane directions.

1. Introduction

Artificially nanostructured materials are attractive platforms since there is an opportunity to tune their magnetic properties by varying their composition, structure, magnetocrystalline and shape anisotropy. Magnetic nanowires are one-dimensional entities in which the magnetization can be forced along the axis of the wire, thanks to shape anisotropy, and these have been investigated since the 1990s for applications in perpendicular magnetic recording [1,2]. Ni and Co nanowires of various diameters have both been widely studied under different deposition conditions [3–8]. It is known that the anisotropy constant of HCP Co is orders of magnitude larger than that of other magnetic materials (e.g. Ni) and forces the magnetization to align along the *c* axis of the crystal [9]. Hence, playing with the crystallographic orientations and the geometrical parameters of the nanowire array (e.g. diameter, length, and spacing), a large variety of magnetic behaviors can be obtained [1,6,7,10] as the coercive field of *c*-axis-oriented HCP Co nanowires is enhanced [11].

For a few decades, many groups have been investigating the electrodeposition of Co nanowires by modifying the pH and the deposition current [11]. However, electrodeposition from aqueous solution is not trivial because of the local pH change at the working electrode. To avoid codeposited impurities, different research groups have considered using organic solutions [12,13] for pure cobalt [14–24] and alloys [25–31]. In the present work, we investigate cobalt electrodeposition from ethylene glycol (EG) solution, a variation of the well-known DES (1ChCl:2EG) where choline chloride, a highly hygroscopic compound with relatively high cost, has been removed and partially replaced by metal precursor salts [32–39]. The possibility of obtaining a high-quality deposit, compact and free of chlorine and/or oxygen has been reported previously by our research group [40,41]. The high concentration of chlorides due to ChCl may be a critical factor due to the intrinsic aggressiveness of the anionic species in solution towards both the electrodeposit and the surrounding environment. Its replacement with chloride salts is thus a valid alternative to guarantee acceptable ionic conductivity but with a lower [Cl^-]. Ethylene glycol (EG) solution containing 0.5 M cobalt chloride salts (approx. 25% [Cl^-] compared with 1ChCl:2EG) was investigated for electrodeposition of both film and nanowires.

* Corresponding author.
E-mail address: luca.magagnin@polimi.it (L. Magagnin).

https://doi.org/10.1016/j.elecom.2019.04.012
Received 15 March 2019; Received in revised form 26 April 2019; Accepted 29 April 2019
Available online 30 April 2019

2. Experimental

Anhydrous ethylene glycol [$C_2H_6O_2$] (Sigma Aldrich, 99.8%) and cobalt chloride salt $CoCl_2{\cdot}6H_2O$ (Sigma Aldrich, ACS reagent, 98%) were used as received. Ethylene glycol was heated to 70 °C, cobalt chloride was added at different concentrations (0.05–0.5 M), and NaCl (Sigma Aldrich, ACS reagent, > 99%) was eventually added as a supporting electrolyte in the frame of electrochemical characterization (0.05 M $CoCl_2$, 0.9 M NaCl). The solution (V = 80 ml) was kept at 70 °C under stirring to avoid water contamination: the vapor pressure of water is much higher than that of ethylene glycol (P°_{H2O} = 5.542 bar, P°_{EG} = 0.064 bar at 70 °C), allowing water evaporation. Solution conductivity was measured at different temperatures (50–90 °C) by means of an AMEL 160 conductivity meter. The electrochemical characterization (AMEL2550) was carried out on an inert substrate (Pt) in a conventional three-electrode electrochemical cell using platinum wires as both quasi-reference (QRE) and counter (CE) electrodes. Cobalt thin films were obtained by means of potentiostatic deposition (PD) on a copper sheet (A ~1.5 × 1.5 cm^2), from −0.75 V vs Pt to −0.95 V vs Pt, using platinum wires and platinized titanium nets as QRE and CE, respectively. The electrodeposited samples were rinsed thoroughly with demi water and subsequently dried under N_2 flux. Cobalt nanowires were synthesized employing an alumina template (0.1 µm Whatman Anodisc) with a copper (~500 nm) seed layer, electrodeposited from a commercial sulfate-based solution, on top of a sputtered gold layer (~50 nm). The thickness of the films was determined both by X-ray fluorescence (XRF) (Fischerscope X-ray XAN) and with an optical profilometer (UBM Microfocus). Cobalt thin films and nanowires were characterized using a Zeiss SUPRA 40 field emission scanning electron microscope (FE-SEM) with in-lens detector and energy dispersive spectroscopy (EDS). The microstructure was investigated by X-ray diffraction with a Philips PW1830 instrument using Cu $K_{\alpha 1}$ radiation (λ = 1.54058 Å). Magnetic characterization was carried out by means of a Vibrating Sample Magnetometer (VSM, model EZ9 by MicroSense LLC).

3. Results and discussion

3.1. Physical and electrochemical characterization

Since ethylene glycol (EG) has negligible conductivity (~10^{-3} mS cm^{-1} at 20 °C), the amount of dissolved salts plays a fundamental role. In fact, the high concentration of chlorides ([Cl^-] > 4.1 M) in traditional deep eutectic solvents (e.g. 1ChCl:2EG) is mainly responsible for the relatively high conductivity of these electrolytes. As reported by Abbott et al., the conductivity of the bare deep eutectic solvents varies from 0.55 mS cm^{-1} (1ChCl:1malonic acid) to 7.61 mS cm^{-1} (1ChCl:2EG) at 20 °C [42]. In the solution under study, such conductivity values (Fig. S1) can be achieved without using choline chloride. Combining a relatively high salt concentration (0.5 M) with a working temperature of 70 °C, a conductivity value of ~7.95 mS cm^{-1} was achieved (Fig. 1). The electrochemical behavior of 0.5 M cobalt chloride solution was investigated on an inert working electrode (Pt), under stagnant conditions. Cobalt reduction at the platinum surface occurred at about −0.7 V vs Pt (Fig. 2a), showing a linear relationship between potential and current density. Although no reduction peak was observed up to −1 V vs Pt, the presence of an anodic peak suggested the formation of a cobalt film during the forward scan, which was subsequently removed (Fig. 2a). Anodic peak position and area were shown to be directly proportional to the lower cathodic limit, resulting in a larger area and a positive shift of the peak position. By extending the potential interval, a reduction peak was found at about −1.25 V vs Pt (Fig. 2a). A further decrease in the lower cathodic limit resulted in secondary reactions: hydrogen evolution was observed for reduction potential < −1.4 V vs Pt where EG deprotonation and/or water electrolysis took place due to atmospheric contamination and salt

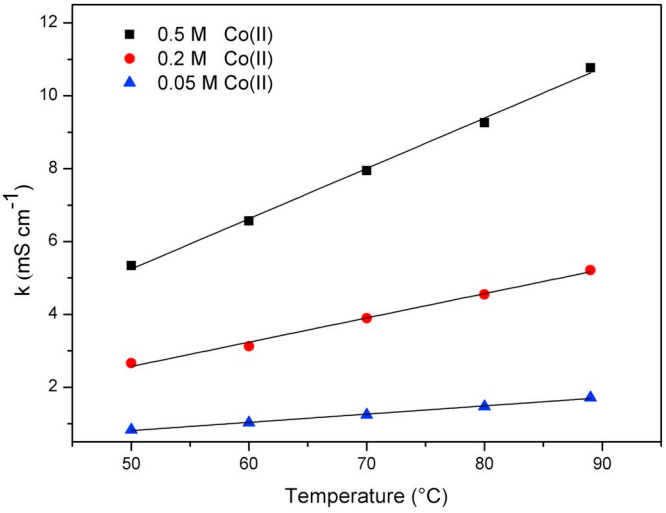

Fig. 1. Conductivity of EG solutions at a different molar concentration of Co(II) chloride salts (0.5 M, 0.2 M, 0.05 M).

hydration. Taking −1 V vs Pt as a cathodic limit, the faradaic efficiency of the cobalt reduction process, calculated from the ratio between anodic and cathodic charge, was around 90%, indicating only a few secondary reactions at the working electrode (Fig. 2b). The diffusion coefficient was studied in a 0.05 M Co(II) solution with 0.9 M NaCl as supporting electrolyte ([Cl^-] = 1 M) since the highly concentrated solution (0.5 M) did not allow clear cathodic peak identification (Fig. S2). By performing CVs at different scan rates, a shift towards more cathodic potentials is shown (Fig. 3). The dependence of cathodic peak potentials on scan rate suggested that the electrochemical reactions involved were irreversible, which is also demonstrated by the wide separation between the cathodic and anodic peaks. According to the Randles–Sevcik equation [43] for an irreversible electrode reaction, the diffusion coefficient D [$cm^2\,s^{-1}$] is linked to the peak current I_p [A] as follows:

$$I_p = 0.495\, nFAC_0(n' + \alpha_{RDS})^{0.5}(F/RT)^{0.5}D_0{}^{0.5}v^{0.5} \quad (1)$$

where n is the number of electrons exchanged in the electrochemical reactions, F is the Faraday constant [C mol^{-1}], A the electrode area [cm^2], C_0 the metal ion concentration [mol cm^{-3}], n' the number of electrons transferred before the rate-determining step (RDS), α_{RDS} is the charge transfer coefficient of the RDS, R the gas constant [8.314 J K^{-1} mol^{-1}], T the absolute temperature [K] and v the scan rate [V s^{-1}]. For an irreversible process n' and α_{RDS} can be defined as follows:

$$|E_p - E_{p/2}| = \frac{1.857\,RT}{(n' + \alpha_{RDS})F} \quad (2)$$

where E_p is the cathodic peak potential [V], $E_{p/2}$ is the cathodic half peak potential corresponding to the potential at half of the peak current. The average ($n' + \alpha_{RDS}$) value reported for the solution considered at 70 °C is 0.5 (Eq. (2)). A diffusion coefficient of D_0 = 2.29 × 10^{-6} $cm^2\,s^{-1}$ at 70 °C was calculated by means of Eq. (1) using the constant slope measured from the $-j_p - v^{0.5}$ graph (Fig. 4). The diffusivity value found is slightly higher than those already reported in the literature for deep eutectic solvents, indicating good physical properties for the solution investigated in this work (Table 1).

3.2. Cobalt morphology and microstructure

Potentiostatic depositions were carried out on copper sheet at high cathodic efficiency (85–90 %): Faraday's law was used, considering a gravimetric approach at a constant deposition charge (10 C), resulting in a film thickness of 1.2–1.4 µm. Morphology dependence on deposition potential is shown in Fig. 5; a clear transition was observed on

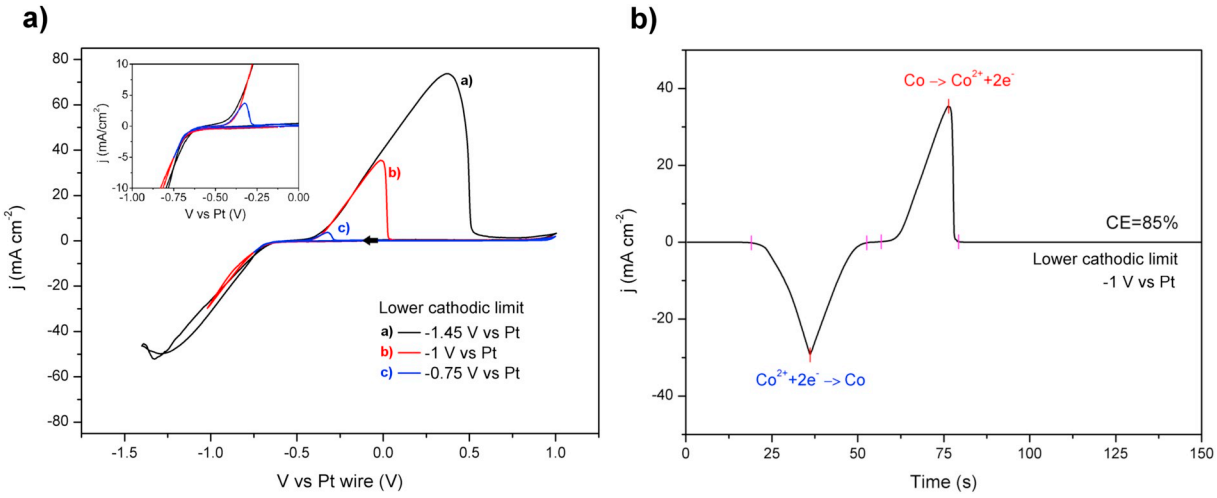

Fig. 2. CV of EG solution with 0.5 M $CoCl_2$ at 70 °C [25 mV s^{-1}]: (a) *j*-V vs Pt plot at different lower cathodic limits. (b) *j*-*t* plot of the corresponding CV with −1 V vs Pt lower cathodic limit.

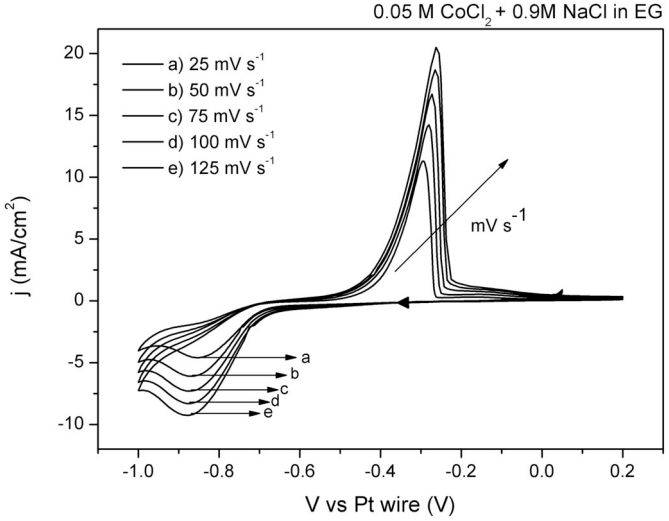

Fig. 3. CV of EG solution with 0.5 M $CoCl_2$ at 70 °C, increasing scan rates [25–125 mV s^{-1}].

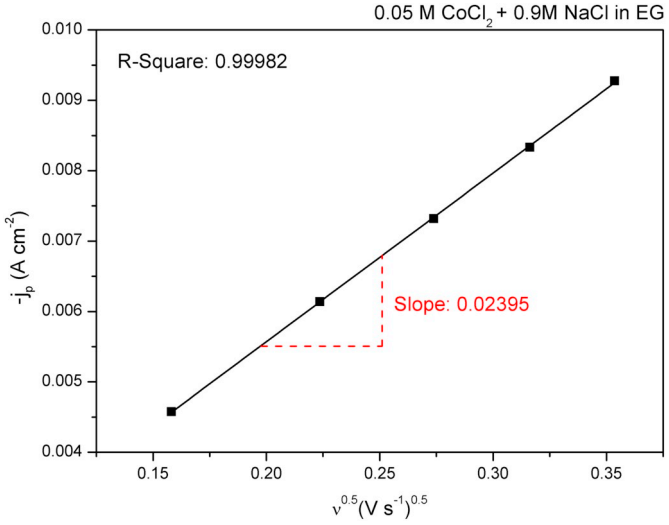

Fig. 4. Cathodic peak current densities of the corresponding CVs (Fig. 3) at different scan rates.

Table 1
Diffusion coefficient values of Co(II) species in different non-aqueous solutions.

Authors	System	T (°C)	D ($cm^2 s^{-1}$)
Yang et al. [14]	$CoCl_2$ in urea-NaBr-KBr	100	2.50×10^{-6}
Carlin et al. [15]	$CoCl_2$ in $AlCl_3$-EMIC	22	4.40×10^{-7}
Su et al. [16]	$Co(BF_4)_2$ in $BMIMBF_4$	60	1.76×10^{-8}
Fukui et al. [17]	$Co(TFSA)_2$ in BMPTFSA	27	7.20×10^{-8}
Li et al. [18]	Co(BF4)2 in BMIMBF4	70	7.60×10^{-8}
Li et al. [19]	$CoCl_2$ in urea-acetamide-LiBr	70	2.20×10^{-6}
Li et al. [20]	$CoCl_2$ in urea-choline chloride	100	1.70×10^{-6}
This work	$CoCl_2$ in ethylene glycol	70	2.29×10^{-6}

increasing the cathodic potential. At the lowest overpotentials, the morphology appeared to be randomly organized with no distinctive features. On increasing the cathodic potential, a transition towards more regular and elongated features was observed. Regardless of the selected deposition potential, compact cobalt films were obtained without any chloride or oxygen contamination detectable through EDS (Fig. 5). Cobalt nanowires were subsequently synthesized using an alumina template (100 nm pores diameter) (Fig. S3a). A plot displaying the current evolution in the first seconds of the process is shown in Fig. S3b: the initial increase in the cathodic current, due to nucleation, is followed by a plateau due to the growth across the membrane. The deposition resulted in the formation of 15–18 μm long nanowires with an aspect ratio of 100–120 (Fig. 6). X-ray diffraction analysis was performed with Bragg–Brentano geometry. The reflection peaks were fitted with a Gaussian function to determine the full width at half maximum (FWHM) and the peak intensity, which are used to determine the average grain size. The cobalt films (Fig. 7a) were shown to have a hexagonal microstructure oriented along the [100] and [101] directions, and a relatively small average grain size (32 nm). In the case of cobalt nanowires, a stronger preferential orientation along the HCP [100] direction is observed (Fig. 7b, Table S1) with no significant variation in the average grain size.

3.3. Magnetic characterization

XRD measurements (Fig. 7b) of the films and nanowires suggested that the *c* axis of the hexagonal cell lies preferentially within the film plane. Hence, the magnetocrystalline anisotropy of the crystal tends to force the magnetization to lie in the plane of the film itself. On the other hand, the shape anisotropy plays opposite roles in thin films and nanowires, favoring an in-plane and an out-of-plane orientation of the magnetization, respectively. Fig. 8a shows that the cobalt film had a

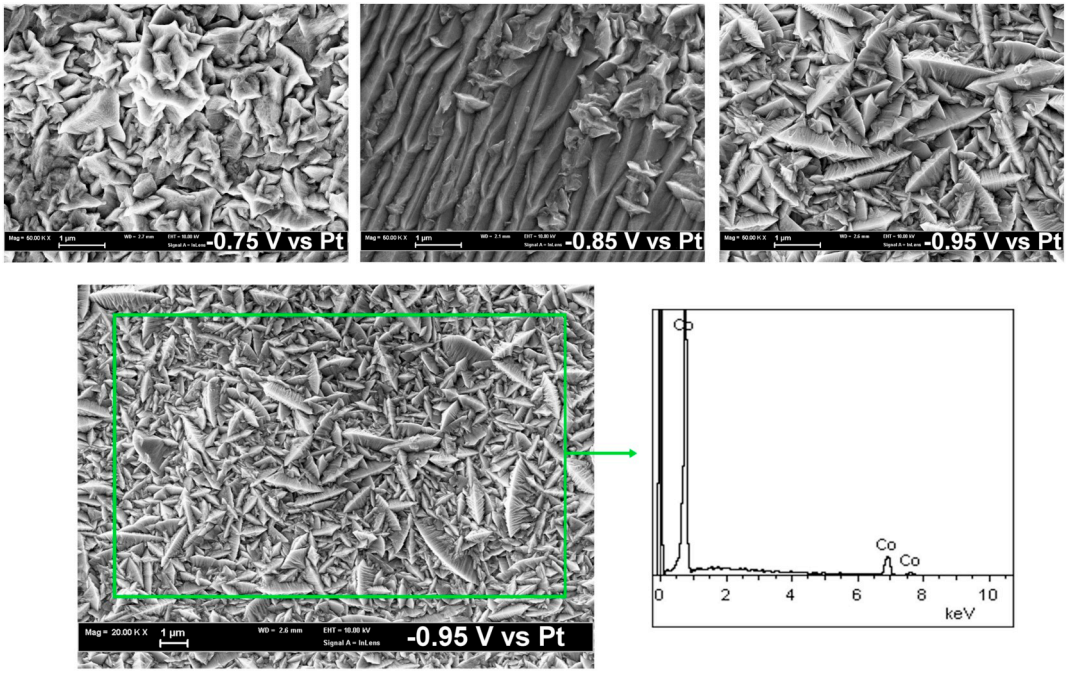

Fig. 5. SEM micrographs of the Co electrodeposits at different cathodic potentials (−0.75 V vs Pt, −0.85 V vs Pt and −0.95 V vs Pt). Higher magnification SEM micrograph and EDS spectrum of the Co electrodeposits at (−0.95 V vs Pt).

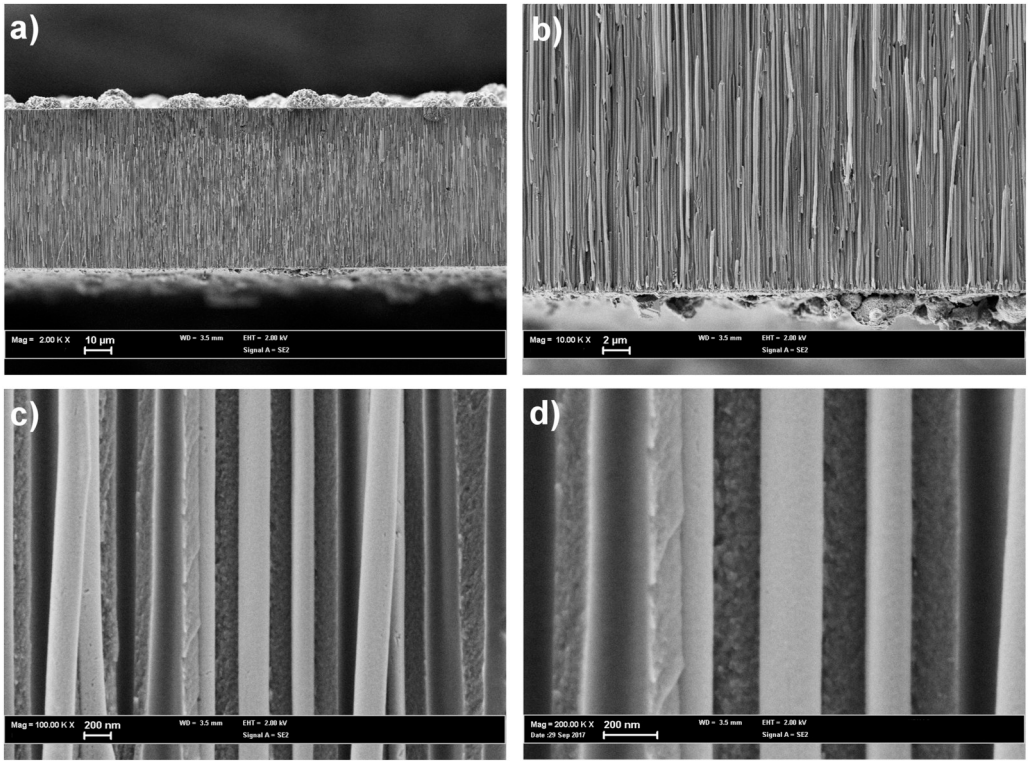

Fig. 6. SEM micrographs of the Co nanowires at −0.95 V vs Pt at 70 °C at different magnifications: (a) 2 kx, (b) 10 kx, (c) 100 kx, (d) 200 kx.

marked in-plane anisotropy, described by an in-plane ($H_{//}$) squared loop while an elongated one is observed when the magnetic field was applied along the normal direction to the film ($H_{\perp}$). For small values of $H_{\perp}$, a relatively small squared hysteresis loop was observed, consistent with the presence of some HCP domains oriented with the *c* axis out of the plane. The situation for nanowires was different: XRD measurements revealed a stronger [100] orientation, favoring an in-plane magnetization. On the other hand, the shape anisotropy would align the magnetization parallel to the wire axis. Co nanowires actually showed similar behavior for both $H_{//}$ and $H_{\perp}$ directions, suggesting that the two anisotropy terms had the same order of magnitude (Fig. 8b) (Table S2). Indeed, the magnetocrystalline anisotropy of HCP Co was characterized by the anisotropy constant $K_1 = 4.5{\cdot}10^5\ \mathrm{J/m^3}$ along the *c* axis. The anisotropy constant of a rod-shaped wire is $K_{\mathrm{wire}} = 1/4\,\mu_0 {M_{\mathrm{sat}}}^2 = 6.4{\cdot}10^5\ \mathrm{J/m^3}$, where $\mu_0 = 4\pi \cdot 10^{-7}\ \mathrm{N/A^2}$ is the vacuum permeability and $M_{\mathrm{sat}} = 1.42{\cdot}10^6\ \mathrm{A/m}$ is the saturation magnetization of

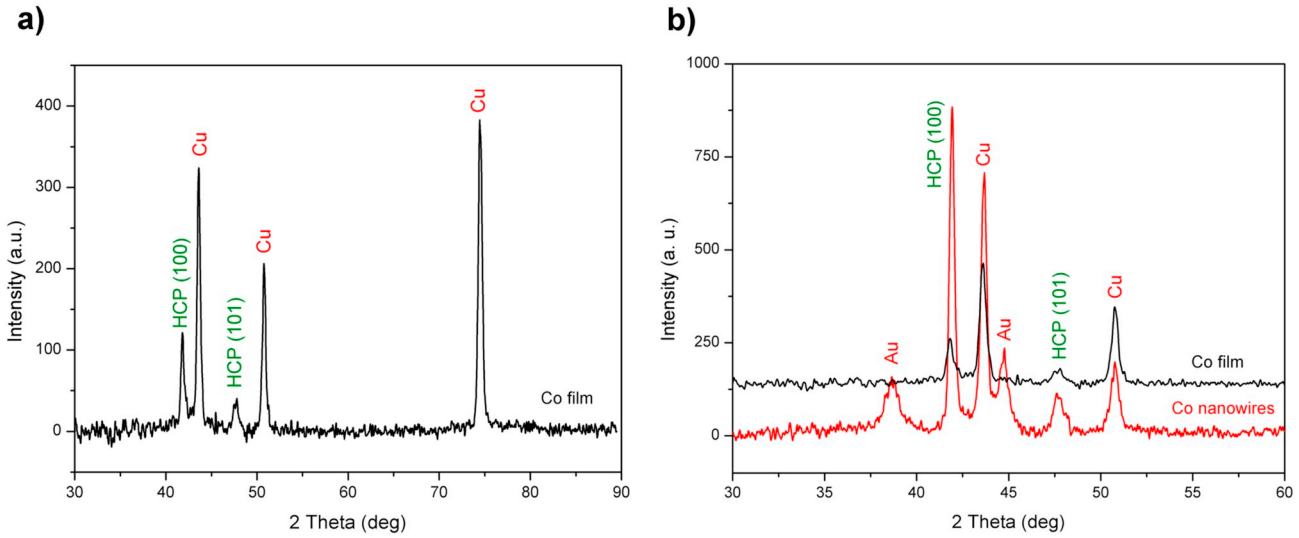

Fig. 7. XRD spectra of Co electrodeposits at −0.95 V vs Pt from 0.5 M Co(II) EG solution: (a) film, (b) film and nanowires.

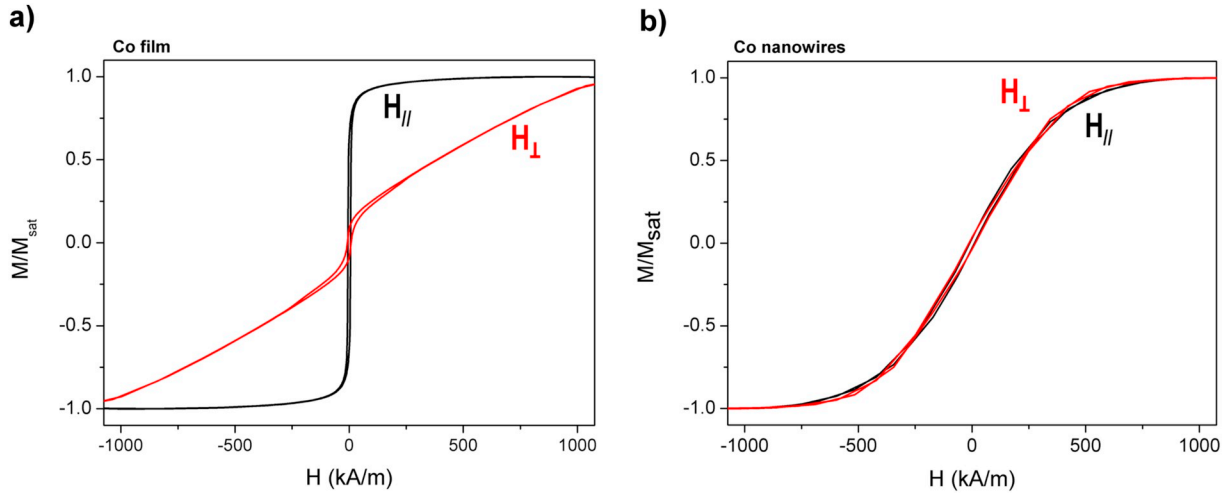

Fig. 8. VSM hysteresis of Co electrodeposits (−0.95 V vs Pt from 0.5 M Co(II) EG solution.): (a) film, (b) nanowires.

cobalt at room temperature [44]. Since K_1 and K_{wire} are of the same order of magnitude, magnetocrystalline and shape contributions compete in orienting the magnetization along two orthogonal directions. The result is compatible with previous studies [8], indicating that magnetic hysteresis loops of cobalt wires with a diameter of the order of 150 nm show the same squareness in-plane and out-of-plane. A reduction in the diameter of the wire would result in an out-of-plane magnetization, but an investigation involving the diameter and aspect ratio of the wires goes beyond the scope of this work.

4. Conclusions

A simple solution based on ethylene glycol is proposed for the electrodeposition of cobalt film and nanowires. Ethylene glycol containing 0.5 M Co(II) had an electrical conductivity of $k = 7.95$ mS cm^{-1}. The cobalt species were estimated to have a diffusion coefficient $D_0 = 2.29 \times 10^{-6}$ cm^2 s^{-1} at 70 °C using the Randles–Sevcik equation. From the cyclic voltammetry investigation and subsequent potentiostatic depositions, the cobalt reduction process occurred with high cathodic efficiency (CE ~85%) indicating the limited presence of secondary reactions. Electron microscopy (SEM) and spectroscopy (EDS) showed compact cobalt films with morphologies dependent on the cathodic potential applied (from −0.75 V vs Pt to −0.95 V vs Pt) but with no traces of contaminants. XRD showed an HCP microstructure with a preferential orientation along the [100] direction, which was particularly evident in the case of Co nanowires. The magnetization of cobalt thin films preferentially lies in the plane of the film, while in the case of nanowires the in-plane and out-of-plane directions display similar behavior. This result was explained in terms of the balance between the magnetocrystalline anisotropy given by the orientation of the crystals and the shape anisotropy due to the one-dimensional structure.

Appendix A. Supplementary data

Supplementary data to this article can be found online at https://doi.org/10.1016/j.elecom.2019.04.012.

References

[1] L. Piraux, J. George, J. Despres, C. Leroy, E. Ferain, R. Legras, K. Ounadjela, A. Fert, Appl. Phys. Lett. 65 (1994) 2484–2486.
[2] G.P. Heydon, S.R. Hoon, A.N. Farley, S.L. Tomlinson, M.S. Valera, K. Attenborough, W. Schwarzacher, J. Phys. D 30 (1997) 1083–1093.
[3] R. Ferré, K. Ounadjela, J.M. George, L. Piraux, S. Dubois, Phys. Rev. B 56 (1997) 14066–14075.
[4] H. Cao, Z. Xu, H. Sang, D. Sheng, C. Tie, Adv. Mater. 13 (2001) 121–123.
[5] M. Darques, A. Encinas, L. Vila, L. Piraux, J. Phys. D 37 (2004) 1411–1416.
[6] J. Qin, J. Nogués, M. Mikhaylova, A. Roig, J.S. Muñoz, M. Muhammed, Chem.

Mater. 17 (2005) 1829–1834.
[7] H. Pan, B. Liu, J. Yi, C. Poh, S. Lim, J. Ding, et al., J. Phys. Chem. B 109 (2005) 3094–3098.
[8] T.M. Whitney, P.C. Searson, J.S. Jiang, C.L. Chien, Science 261 (1993) 1316–1319.
[9] W. Sucksmith, J.E. Thompson, Proc. R. Soc. Lond. A 225 (1954) 362–375.
[10] A.K.M. Bantu, J. Rivas, G. Zaragoza, M.A. López-Quintela, M.C. Blanco, J. Appl. Phys. 89 (2001) 3393–3397.
[11] M. Darques, L. Piraux, A. Encinas, P. Bayle-Guillemaud, A. Popa, U. Ebels, Appl. Phys. Lett. 86 (2005) 072508.
[12] T. Welton, Chem. Rev. 99 (1999) 2071–2084.
[13] A.P. Abbott, K.J. McKenzie, Phys. Chem. Chem. Phys. 8 (2006) 4265–4279.
[14] Q.Q. Yang, K.R. Qui, D.R. Zhu, L.C. Sa, Electrochemistry 1 (1995) 274–277.
[15] R.T. Carlin, H.C. De Long, J. Fuller, P.C. Trulove, J. Electrochem. Soc. 145 (1998) 1598–1607.
[16] C. Su, M. An, P. Yang, H. Gu, X. Guo, Appl. Surf. Sci. 256 (2010) 4888–4893.
[17] R. Fukui, Y. Katayama, T. Miura, Electrochim. Acta 56 (2011) 1190–1196.
[18] M. Li, Z. Wang, R.G. Reddy, EPD Congress, (2014), pp. 241–250.
[19] M. Li, B. Gao, Z. Shi, X. Hu, S. Wang, L. Li, Z. Wang, J. Yu, J. Solid State Electrochem. 20 (2016) 247–254.
[20] M. Li, Z. Wang, R.G. Reddy, Electrochim. Acta 123 (2014) 325–331.
[21] T. Le Manh, E.M. Arce-Estrada, I. Mejía-Caballero, J. Aldana-González, M. Romero-Romo, M. Palomar-Pardavé, J. Electrochem. Soc. 165 (2018) D285–D290.
[22] J. Sniekers, P. Geysens, T. Vander Hoogerstraete, L. Van Meervelt, J. Fransaer, K. Binnemans, Dalton Trans. 47 (2018) 4975–4986.
[23] A.M. Sakita, R. Della Noce, C.S. Fugivara, A.V. Benedetti, Phys. Chem. Chem. Phys. 18 (2016) 25048–25057.
[24] G. Panzeri, L. Pedrazzetti, C. Rinaldi, L. Nobili, L. Magagnin, J. Electrochem. Soc. 165 (2018) D580–D583.
[25] P. Cojocaru, L. Magagnin, E. Gomez, E. Vallés, Mater. Lett. 65 (2011) 3597–3600.
[26] P. Guillamat, M. Cortés, E. Vallés, E. Gómez, Surf. Coat. Technol. 206 (2012) 4439–4448.
[27] G. Panzeri, M. Tresoldi, C. Rinaldi, L. Magagnin, J. Electrochem. Soc. 164 (2017) D930–D933.
[28] N.M. Pereira, C.T. Sousa, C.M. Pereira, J.P. Araújo, A.F. Silva, Cryst. Growth Des. 17 (2017) 5208–5215.
[29] G. Saravanan, S. Mohan, J. Alloys Compd. 522 (2012) 162–166.
[30] J. Vijayakumar, S. Mohan, S.A. Kumar, S. Suseendiran, S. Pavithra, Int. J. Hydrog. Energy 38 (2013) 10208–10214.
[31] L. Anicai, S. Costovici, A. Cojocaru, A. Manea, T. Visan, Trans. IMF 93 (2015) 302–312.
[32] S. Pawar, A. Moholkar, K. Rajpure, C. Bhosale, Appl. Surf. Sci. 253 (2007) 7313–7317.
[33] J. Wellings, A. Samantilleke, S. Heavens, P. Warren, I. Dharmadasa, Sol. Energy Mater. Sol. Cells 93 (2009) 1518–1523.
[34] T. Vorobyova, O. Vrublevskaya, Surf. Coat. Technol. 204 (2010) 1314–1318.
[35] H.P. Nguyen, M. Wu, J. Su, R.J. Vullers, P.M. Vereecken, J. Fransaer, Electrochim. Acta 68 (2012) 9–17.
[36] M. Wu, H.P. Nguyen, R.J. Vullers, P.M. Vereecken, K. Binnemans, J. Fransaer, J. Electrochem. Soc. 160 (2013) D196–D201.
[37] M. Wu, K. Binnemans, J. Fransaer, Electrochim. Acta 147 (2014) 451–459.
[38] H. Maltanava, T. Vorobyova, O. Vrublevskaya, Surf. Coat. Technol. 254 (2014) 388–397.
[39] M. Pallaro, F. Moretto, G. Panzeri, L. Magagnin, Trans. IMF 96 (2018) 265–268.
[40] G. Panzeri, A. Accogli, E. Gibertini, C. Rinaldi, L. Nobili, L. Magagnin, Electrochim. Acta 271 (2018) 576–581.
[41] G. Panzeri, D. Muller, A. Accogli, E. Gibertini, E. Mauri, F. Rossi, L. Nobili, L. Magagnin, Electrochim. Acta 296 (2019) 465–472.
[42] A.P. Abbott, R.C. Harris, K.S. Ryder, J. Phys. Chem. B 111 (2007) 4910–4913.
[43] C. Batchelor-McAuley, E. Kätelhön, E.O. Barnes, R.G. Compton, E. Laborda, A. Molina, ChemistryOpen 4 (2015) 224–260.
[44] R.M. Bozorth, Ferromagnetism, Wiley-VCH, 1993.